lubricants

MDPI

Article

Synergistic Lubrication and Anti-Corrosion Effects of Benzotriazole and Ionic Liquid Under Current-Carrying Friction

Taiyu Su [1,2,3], Kun Peng [4], Duo Zhang [5], Luyi Sun [1], Yuxin Chen [1], Yiheng Yu [1] and Ming Zhou [1,2,3,*]

[1] School of Mechanical and Automotive Engineering, Guangxi University of Science and Technology, Liuzhou 545006, China
[2] Guangxi Earthmoving Machinery Collaborative Innovation Center, Guangxi University of Science and Technology, Liuzhou 545006, China
[3] Guangxi Tsinglube New Material Technology Co., Ltd., Liuzhou 545006, China
[4] Guangxi Jianxing Guangyin New Material Technology Co., Ltd., Nanning 530024, China
[5] School of Medicine, Guangxi University of Science and Technology, Liuzhou 545006, China
* Correspondence: zhoum03@163.com

Abstract: The corrosive nature of ionic liquids (ILs) limits their potential as high-performance conductive lubricants in practical engineering applications. This study systematically investigates the effects of benzotriazole (BTA) as a corrosion inhibitor on the lubricating performance of ILs at different concentrations and applied currents, along with the underlying mechanisms. In the 0.5–5 A current range, BTA effectively reduces friction, wear, and arc erosion damage to the friction surface. As the applied current increases, the BTA-Fe reaction film suppresses oxide formation, thereby reducing electrical contact resistance (ECR). Moreover, the effectiveness of BTA is concentration-dependent: at 0.5 A and a BTA concentration of 0.5 wt%, the coefficient of friction (COF) decreases by 16.5%, and wear volume is reduced by 53.4%. Friction testing and surface analysis show that the BTA-IL combination exhibits synergistic lubrication and anti-corrosion effects under current-carrying conditions, with varying wear and lubrication mechanisms depending on the applied current.

Keywords: ionic liquid; benzotriazole; corrosion inhibitor; current-carrying friction

check for updates

Received: 6 December 2024
Revised: 5 February 2025
Accepted: 6 February 2025
Published: 11 February 2025

Citation: Su, T.; Peng, K.; Zhang, D.; Sun, L.; Chen, Y.; Yu, Y.; Zhou, M. Synergistic Lubrication and Anti-Corrosion Effects of Benzotriazole and Ionic Liquid Under Current-Carrying Friction. *Lubricants* **2025**, *13*, 77. https://doi.org/10.3390/lubricants13020077

Copyright: © 2025 by the authors. Licensee MDPI, Basel, Switzerland. This article is an open access article distributed under the terms and conditions of the Creative Commons Attribution (CC BY) license (https://creativecommons.org/licenses/by/4.0/).

1. Introduction

The continuous advancement of modern industry has led to the widespread use of electrical contacts, particularly in high-end electronic devices, electric vehicles, and power transmission systems. Electrical contact components are critical in many types of electrical equipment because they perform essential functions such as motion transmission, switch control, and current conduction. The reliability and stability of the equipment are closely tied to the performance of these components [1,2]. Friction and wear are key factors contributing to the failure of electrical contact components. Under current-carrying friction conditions, micro gaps present between friction pairs are conducive to arc generation, and arc-induced electrical erosion typically leads to more severe wear than conventional physical friction [3–5]. Therefore, enhancing the lubrication performance and current-carrying capacity of current-carrying friction pairs is critical to realize the stable operation of electrical contact components. Although various metal-based self-lubricating materials have been extensively studied to improve the electrical conductivity and tribological properties of friction pairs, several challenges persist. For example, under high-current conditions, the wear resistance of metal-based self-lubricating materials is often limited,

which leads to increased wear and reduced lifespan. Further, certain conductive materials may negatively impact lubrication performance due to insufficient hardness and/or other physical properties, making it challenging to achieve a balance between conductivity and effective lubrication. Finally, the stability and compatibility of these materials under different environmental conditions require further investigation [6–8]. Developing high-performance lubricants is essential for addressing these challenges. These lubricants must not only exhibit superior lubrication properties but also possess adequate electrical conductivity to fulfill the specific requirements of electrical contact components.

Lubricants are widely used in industrial applications to reduce friction and wear. Traditional lubricants rely on protective films, such as physically adsorbed layers and/or tribochemical reaction films, to ensure lubricity. However, these protective films composed of oil films, oxides, or tribochemical reaction products exhibit poor electrical conductivity, resulting in rapid heating and thermal accumulation at contact interfaces subjected to electric currents, which can negatively affect the performance of the lubricant. In contrast, conductive lubricants form current pathways at the friction interface to suppress arc generation while effectively reducing electrical contact resistance [9]. Commonly studied types of conductive lubricants include ionic liquids (ILs), metal nanoparticles, conductive polymers, and carbon-based materials [10–13]. ILs were first introduced as a novel lubricant with promising potential in 2001, and have since garnered considerable attention in the field of tribology research [14]. They possess a range of excellent properties, including superior lubricity and electrical conductivity, extremely low volatility, thermal stability, and tunable designability [15–18]. These properties provide significant advantages when using ILs as conductive lubricants in industrial applications. However, the inherent corrosiveness of most IL lubricants poses a challenge because they can lead to corrosive wear of the friction pair materials. This corrosiveness can be attributed to the hydrolysis of fluorine-containing anions and other halogen impurities during the friction process [19,20]. Wijanarko et al. [21] observed that the tribocorrosive effects of IL lubricants can lead to the formation of unstable passivation/friction films, subsequently resulting in high friction and wear. Therefore, various strategies have been employed to mitigate the corrosive effects of ILs during friction processes. Cao et al. [22] broadly categorized these strategies into the following three types: (1) adding corrosion inhibitors to ILs; (2) developing functionalized ILs; and (3) using ILs as additives in lubricating oils or greases.

Benzotriazole (BTA) is a widely used industrial corrosion inhibitor that has attracted considerable attention because of its potential to mitigate the tribocorrosive behaviors of IL. Liu et al. [23] combined BTA with an IL using ultrasonic assistance to produce a composite lubricant that effectively mitigated the corrosiveness of the IL and demonstrated excellent tribological performance in both copper–copper and steel–steel friction pairs. Their analysis indicated that BTA formed a chemical bond with metal atoms through the sp^2-hybridized orbital electrons of its N atoms to create a dense chemisorbed protective film on the metal surface that prevented the IL from corroding the metal. Cai et al. [24] synthesized imidazolium-based functionalized ILs containing BTA groups with various anion types, including $BF4^-$, $PF6^-$, and $NTF2^-$. The results indicate that ILs functionalized with BTA groups exhibit superior anti-corrosion performance compared to ILs without BTA groups and effectively reduce friction and wear when used as additives in grease lubrication. Yu et al. [25,26] used lignin, tetrabutylphosphorus, and BTA as raw materials to synthesize a novel IL containing BTA groups. The experimental results demonstrate that the ILs functionalized with BTA groups exhibit superior lubrication performance and effectively inhibit water-induced corrosion of iron when utilized as additives in water-based lubricants.

However, these aforementioned studies were conducted under zero-current conditions, which are considerably different from the current-carrying friction conditions encountered

in practical electrical contact component applications. Critically, current-carrying tribology, in which electrical factors are coupled with frictional factors, is considerably more complex than conventional friction-only tribology. The electrochemical erosion and reactions induced by the passing of current through the friction interface, as well as its effect on the physical and chemical properties of the lubricants, increase the complexity of the tribological system. These factors can not only alter the damage mechanisms of the friction pair materials but also affect the redox processes and change the viscosity characteristics of the lubricant, thereby affecting the overall lubrication performance. Therefore, to expand the application of ILs as conductive lubricants in practical engineering, the action mechanism of BTA as a corrosion inhibitor under current-carrying friction conditions requires further investigation and clarification.

This study established a current-carrying friction test system, comprising a friction tester and current application device to simulate actual electrical contact environments. We systematically varied BTA concentration and applied current intensity to investigate the coefficient of friction (COF), electrical contact resistance (ECR), and wear behavior using fluorine-containing imidazolium IL (1-butyl-3-methylimidazolium hexafluorophosphate) as the base lubricant and BTA as an additive. Wear surfaces were characterized by scanning electron microscopy (SEM), energy-dispersive spectroscopy (EDS), X-ray photoelectron spectroscopy (XPS), and Raman spectroscopy. Additionally, an elemental ratio analysis was conducted to explore the lubrication and corrosion inhibition mechanisms of BTA as an IL additive under current-carrying conditions. Our findings provide new insights into the synergistic lubrication and anti-corrosion effects of BTA and IL in current-carrying friction scenarios. This contributes to a fundamental understanding of lubricants for sliding electrical contacts and provides broader implications for developing advanced scalable lubricants, as well as more robust, energy-efficient, and cost-effective electrical systems.

2. Materials and Methods

2.1. Materials

1-butyl-3-methylimidazolium hexafluorophosphate (99% purity) purchased from the Lanzhou Institute of Chemical Physics, Chinese Academy of Sciences (Lanzhou, China) was used as the IL in these experiments. The BTA (1H-Benzotriazole) was obtained from Macklin Biochemical Co., Ltd. (Shanghai, China). Petroleum ether was sourced from Sichuan Xilong Science Co., Ltd. (Chengdu, China) and ethanol was acquired from Chengdu Cologne Chemicals Co., Ltd. (Chengdu, China). All reagents were of analytical grade. Steel balls (GCr15; 6.35 mm diameter; HRC62 hardness) were purchased from Yasteel Co., Ltd. (Heze, China), and steel plates (GCr15; 40 $\times$ 30 $\times$ 5 mm; HRC50 hardness) were purchased from Suzhou Zetian Precision Metal Co., Ltd. (Suzhou, China). The required composite lubricants were prepared by applying ultrasonic excitation to thoroughly dissolved BTA mass fractions of 0.1, 0.5, 1, 2, and 5 wt% in the IL.

2.2. Characterization of the Lubricants

The electrochemical corrosion tests of the lubricants were conducted using a SHI660E electrochemical workstation, employing a conventional three-electrode system: a platinum sheet as the counter electrode, a saturated calomel electrode as the reference electrode, and GCr15 steel as the working electrode. The electrolyte was an ionic liquid containing different concentrations of BTA. Potentiodynamic polarization tests were performed within an open-circuit potential (OCP) range of $\pm$300 mV at a scan rate of 5 mV/s to obtain Tafel curves. The electrochemical parameters were calculated using the Tafel extrapolation method to evaluate the effect of different BTA concentrations on corrosion performance. The chemical structure of the lubricants was characterized using a Thermo Scientific Nicolet

Summit X Fourier-transform infrared (FTIR) spectrometer (Thermo Fisher, Waltham, MA, USA), with scanning performed over a wavenumber range of 4000–500 cm^{-1} to analyze the infrared spectra of ionic liquids with varying BTA concentrations.

2.3. Tribological Tests

The tribological performance of each lubricant under different applied electrical currents was evaluated using a steel ball–plate friction pair on a Bruker UMT-TriboLab multifunctional tribometer (Bruker, Karlsruhe, Germany). Figure 1 illustrates a schematic representation of the experimental setup. During the experiment, a constant current was supplied by an ITECH IT6700 power source (ITECH, Nanjing, China), and the voltage across the friction pair was measured in real time using a KEYS Company Keysight 34450A 5 1/2 digital multimeter (KEYS, Santa Rosa, CA, USA). The tribological tests used GCr15 bearing steel for both the ball and the plate, simulating current-carrying friction conditions relevant to bearing components in electrical equipment. The tests were performed under a normal load of 10 N, with a reciprocating amplitude of 3 mm and a frequency of 5 Hz, for a duration of 20 min. Electrical currents of 0, 0.5, 2, 3.5, and 5 A were externally applied to systematically analyze the tribological performance under different current conditions. To ensure reliability, a minimum of three tribological tests were performed for each set of parameters. The standard deviation was calculated based on repeated measurements and presented as error bars in the figures to reflect the degree of variability in repeated measurements. The effect of surface roughness was eliminated by mechanically polishing each steel plate to a roughness of ~10 nm before testing. All tribological tests were conducted in a laboratory environment at an ambient temperature of 25 ± 2 °C and a relative humidity of 40 ± 10%. Prior to each test, the steel ball and plate were subjected to ultrasonic cleaning with petroleum ether and anhydrous ethanol for 10 min to eliminate surface impurities. Subsequently, ~0.5 g of the desired lubricant was applied to the friction area using a pipette. The COF and contact voltage were automatically logged by a computer during the tests. Following each friction test, the ECR of the friction pair was determined using Ohm's law, assuming that the resistances of the wires, components, and other system elements remained unchanged.

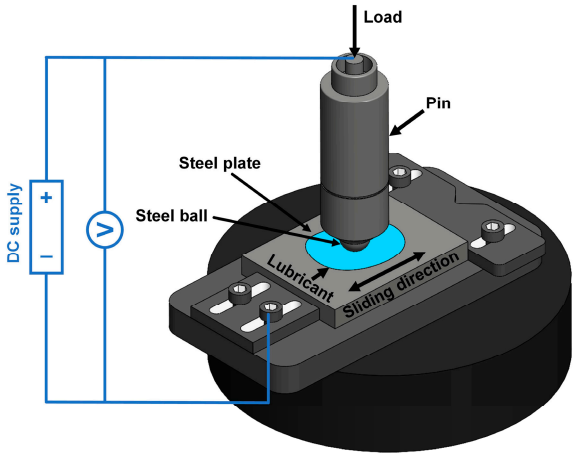

Figure 1. Schematic representation of the experimental setup.

2.4. Surface Analysis

The wear scars on the surfaces of the steel ball and plate were observed using a Zeiss Axioscope 5 research-grade upright material microscope (Zeiss, Oberkochen, Germany). The morphologies and profiles of the wear scars were obtained using a Bruker NPFLEX three-dimensional white-light interferometer, and the wear volume was automatically calculated by the device to quantify the extent of wear. In addition, the steel plate was cut

into 1 cm × 1 cm squares using wire-cutting technology for SEM, EDS, and XPS testing. The microstructural features of the wear scars were studied using a Carl Zeiss SIGMA SEM at an acceleration voltage of 20 kV. EDS analysis was performed on the same SEM equipment. The elemental composition and relative content on the worn surfaces were analyzed using a Thermo Scientific K-α X-ray photoelectron spectrometer, with a spot diameter ranging from 100 to 200 μm. Finally, the material composition of the worn surfaces was further analyzed using a Horiba XploRA Raman spectrometer (Horiba XploRA, Kyoto, Japan) equipped with a 532 nm laser and a scanning range of 400–2000 cm^{-1}.

3. Results and Discussion

3.1. Physicochemical Properties of the Lubricants

To evaluate the corrosion inhibition performance of BTA in the ionic liquid corrosion environment, Tafel curves were obtained through potentiodynamic polarization tests, as shown in Figure 2. Electrochemical parameters derived from the Tafel curves, including corrosion potential (E_{corr}), corrosion current density (i_{corr}), cathodic Tafel slope (β_c), and anodic Tafel slope (β_a), are presented in Table 1. The experimental results indicate that the corrosion potential shifts positively with the addition of different concentrations of BTA, suggesting a reduced tendency for metal corrosion. When the BTA concentration is 0.1 wt%, the corrosion current density decreases slightly, but the inhibition effect is relatively limited. As the concentration increases to the range of 0.5–2 wt%, the corrosion current density decreases significantly, particularly at 1 wt%, where it drops by two orders of magnitude. This indicates that within this concentration range, BTA molecules can effectively adsorb onto the metal surface, forming a dense and stable protective film that suppresses metal dissolution and corrosion. At a concentration of 5 wt%, the reduction in corrosion current density tends to plateau, indicating that the inhibition effect of BTA may reach saturation at high concentrations, and further increases in concentration have limited additional impact on improving corrosion behavior. The changes in Tafel slopes further reveal the mechanism by which BTA influences the corrosion reaction. With increasing BTA concentration, the cathodic Tafel slope shows a continuous increase, indicating that BTA effectively inhibits the cathodic reaction. This may be attributed to the adsorption of BTA molecules on the metal surface, reducing the number of active sites for the cathodic reaction and impeding electron transfer. In contrast, the anodic Tafel slope reaches its maximum at 0.1 wt% and then gradually decreases within the range of 0.5–5 wt%. This trend may be due to the following reasons: at low concentrations, BTA molecules initially adsorb onto the metal surface, effectively covering active sites for the anodic reaction and significantly suppressing metal dissolution. However, at higher concentrations, excessive adsorption of BTA may lead to uneven protective film structures or localized desorption, reducing the stability of the protective film and thereby weakening its inhibition of the anodic reaction. In summary, under the ionic liquid corrosion environment, BTA effectively inhibits the metal corrosion process by forming a dense protective film through adsorption on the metal surface. Furthermore, its corrosion inhibition performance demonstrates a clear dependence on concentration.

The ionic liquid lubricants with varying BTA concentrations were characterized using an FTIR spectrometer to investigate the potential impact of BTA on the molecular structure of the ionic liquid. The results are shown in Figure 3. After adding BTA, the intensities of the absorption peaks exhibited no significant changes. The peak around 3168 cm^{-1} corresponds to the stretching vibration mode of the C-H bond on the imidazole ring. The peaks at 2966 cm^{-1} and 2873 cm^{-1} are primarily attributed to the stretching vibration modes of C-H bonds on the butyl and methyl side chains. The absorption peaks at 1617 cm^{-1} and 1575 cm^{-1} are assigned to the stretching vibrations of C=C and C=N bonds in the

imidazole ring framework. The absorption peak at 1467 cm^{-1} is mainly associated with the deformation vibration of the methyl C-H bond. The peak at 1167 cm^{-1} corresponds to the stretching vibration of the C-N bond in the imidazole ring framework. The peak at 822 cm^{-1} is a characteristic of the P-F stretching vibration in the hexafluorophosphate anion, while the absorption peak at 746 cm^{-1} is primarily related to various in-plane bending vibration modes of C-H bonds. When different concentrations of BTA were added to the IL, the infrared characteristics of the resulting mixture did not show significant changes. Due to the low doping concentration of BTA, its characteristic absorption peaks may overlap with the strong absorption peaks of the IL. However, slight shifts were observed in the P-F stretching vibration peak of the hexafluorophosphate anion and the C-H stretching vibration peak at 746 cm^{-1} in the IL. These shifts suggest that the nitrogen atoms and aromatic rings in BTA molecules may interact with the cations or anions of the IL through hydrogen bonding or π-π interactions, altering the intermolecular forces in the system. Moreover, the absorption peaks associated with the imidazole ring framework of the IL showed no significant shifts, indicating that BTA, at mass fractions of 5 wt% or lower, primarily influences certain physical properties of the IL by forming secondary bonds (e.g., hydrogen bonds, π-π interactions) rather than directly altering the primary structure or functional groups of the IL molecules.

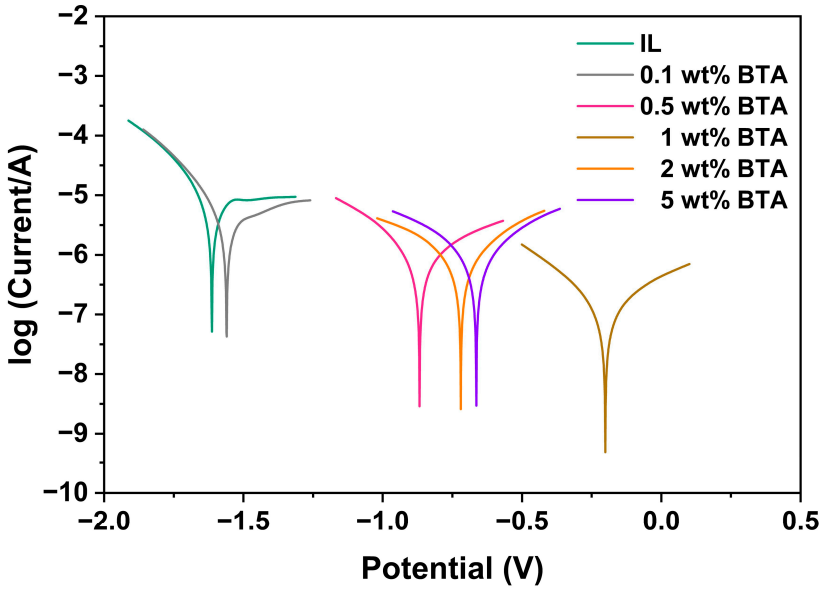

Figure 2. Tafel curves of GCr15 steel in ionic liquid with and without BTA.

Table 1. Electrochemical parameters of GCr15 steel in ionic liquid with and without BTA.

Sample	E_{corr} (V)	i_{corr} (μA·cm^{-2})	β_c (mV·dec^{-1})	β_a (mV·dec^{-1})	Corrosion Rate (mm·$Year^{-1}$)
IL	−1.616	3.99	−143	295	0.0462
0.1 wt% BTA	−1.563	3.28	−141	584	0.0381
0.5 wt% BTA	−0.867	0.47	−165	221	0.0054
1 wt% BTA	−0.201	0.07	−171	211	0.0008
2 wt% BTA	−0.719	0.42	−199	187	0.0049
5 wt% BTA	−0.664	0.48	−189	190	0.0056

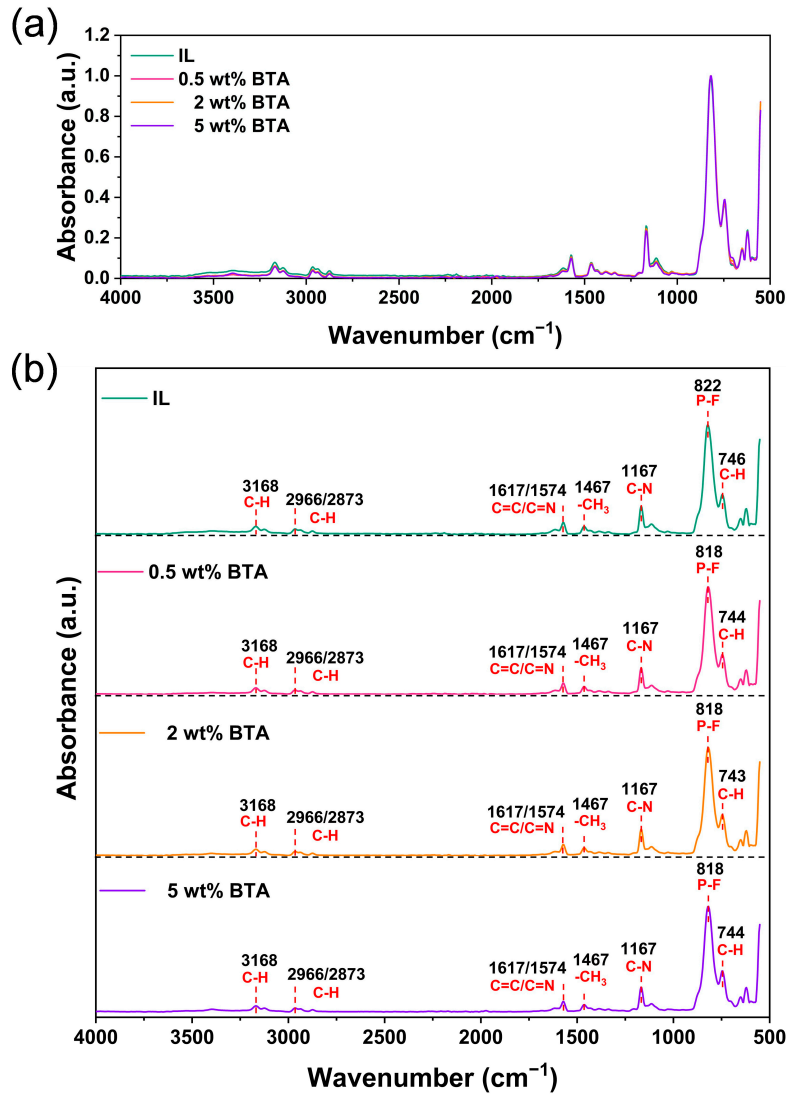

Figure 3. Infrared spectra of ionic liquid containing varying concentrations of BTA: (**a**) comparison of absorption intensities; (**b**) comparison of peak positions.

3.2. Tribology Behaviors and Wear Scar Morphologies

3.2.1. Effect of Lubrication Condition

Figure 4 presents a comparison of the COF and ECR measured under various lubrication conditions with an applied current of 0.5 A. The COF curves for dry friction, IL lubrication, and 0.5 wt% BTA lubrication are shown in Figure 4a. The highest COF is observed for dry friction, with an average value of 0.52. Under IL lubrication, the COF significantly decreased to an average of 0.085. With the addition of 0.5 wt% BTA, the COF decreased further to 0.071, representing a 16.5% reduction compared to that of IL lubrication. The corresponding ECRs under these conditions are shown in Figure 4b, which exhibit an inverse trend to that of the COF. Figure 4c,d display the cross-sectional profiles of the wear scars and corresponding wear volumes for each of the three lubrication conditions. The wear volume trend mirrored that of the COF. In dry friction, the friction pair surfaces were in direct contact, hindering the formation of an effective lubricating film at the interface, which leads to high friction and wear. Compared to dry friction, IL as a lubricant filled the friction interface, significantly reducing frictional wear. The wear volume under IL lubrication was 0.8293×10^5 μm^3, which is only 1/15 of that in dry friction. The ECR is considered an indicator of the presence and state of the surface film at the friction interface [27]. ECR under IL lubrication was higher than that in dry friction, which implies

that an effective non-conductive lubricating film may have formed at the interface. Under 0.5 wt% BTA lubrication, the wear volume decreased to 0.3864 × 10^5 μm^3, representing a 53.4% reduction compared to that under IL lubrication, while the ECR increased. This implies that the addition of BTA may have increased the thickness of the non-conductive lubricating film or promoted the formation of a more stable film.

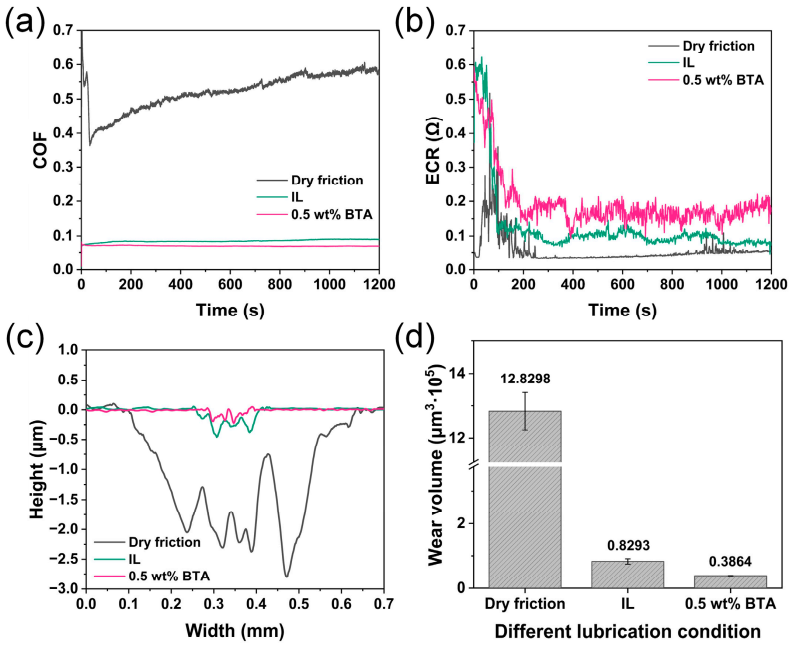

Figure 4. Tribological behaviors obtained under different lubrication conditions at 0.5 A: (**a**) coefficients of friction, (**b**) electrical contact resistances, (**c**) cross-sectional profile of the wear scars, and (**d**) wear volumes.

Figure 5 compares the optical microscopic morphologies of the worn surfaces of steel balls and plates under different lubrication conditions at an applied current of 0.5 A. Figure 5a,d show the optical microscope images after dry friction. Clear material spalling pits were observed on the worn surface of the plate, and a significant amount of oxide adhesion and material transfer was evident on the worn surface of the ball. During dry friction, the material near the contact points between the steel ball and plate undergoes shearing and detachment under the action of frictional force. The accumulation of significant frictional heat and residual wear debris on the friction surface further exacerbates surface damage, resulting in high friction and severe wear. Figure 5b,e present the optical microscope images under IL lubrication. Compared to dry friction, the wear scar width under IL lubrication is significantly reduced, and no obvious oxide accumulation or material transfer is observed on the surfaces of the steel ball or plate. This implies that IL lubrication effectively reduces material detachment and surface damage during friction. Further, the presence of a lubricating film effectively lowers frictional heat, preventing the high-temperature oxidation and wear that is typically observed in dry friction. Finally, Figure 5c,f display the optical microscope images under 0.5 wt% BTA lubrication. Compared with pure IL lubrication, the addition of BTA further reduces the wear scar width, which results in a smoother wear surface. These results indicate that IL as a conductive lubricant effectively alleviates material oxidation and transfer issues in dry friction. Moreover, the incorporation of BTA enhances the anti-friction and anti-corrosion properties of the IL lubricant, producing smoother wear surfaces and significantly reducing wear.

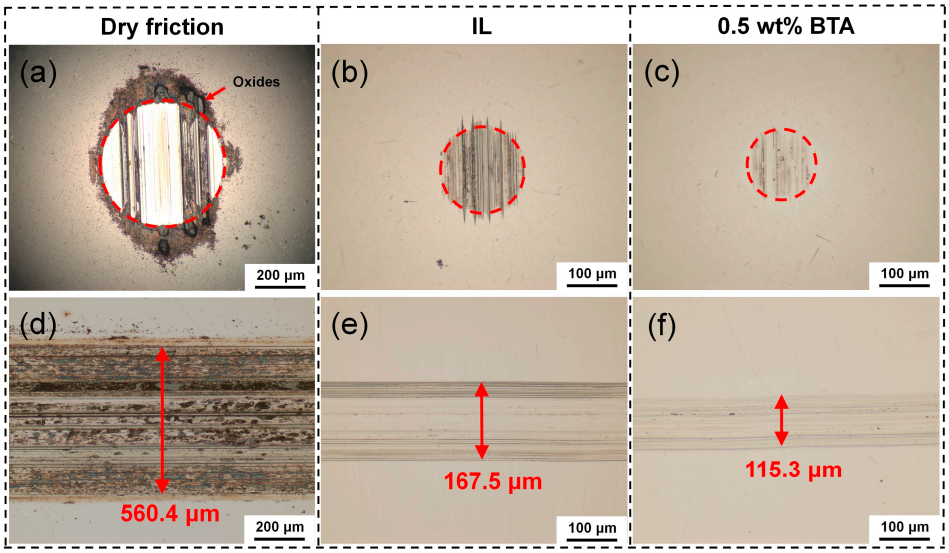

Figure 5. Optical micrographs of worn surfaces on the steel ball and plate at a current of 0.5 A after: (**a**,**d**) dry friction, (**b**,**e**) pure IL lubrication, and (**c**,**f**) 0.5 wt% BTA lubrication.

3.2.2. Effect of BTA Concentration

The effects of BTA concentration on the COF and ECR are examined in detail to optimize the performance of the IL lubricant. Figure 6a,d, respectively, show the COF curves and corresponding average COF for different BTA mass fractions added to the IL. The average COF reached its lowest value of 0.0714 at 0.5 wt%, and then it increased with a further increase in concentration, reaching a maximum of 0.0767 at 5 wt%. Figure 6b,e illustrate the cross-sectional profiles of wear scars and the corresponding wear volumes under different BTA concentrations. The trend in wear volume mirrored that of the COF, with the smallest wear observed at 0.5 wt%. When the BTA concentration reached 5 wt%, the wear volume increased by ~1.3 times compared to the minimum value, indicating that excessively high BTA concentrations led to severe wear. At a 0.1 wt% BTA concentration, the additive content was too low to provide ideal lubrication performance. Although higher concentrations such as 1 and 5 wt% were used, excessive amounts of the additive likely led to the formation of a lubricating film that was loose and unstable, thereby reducing its lubrication performance.

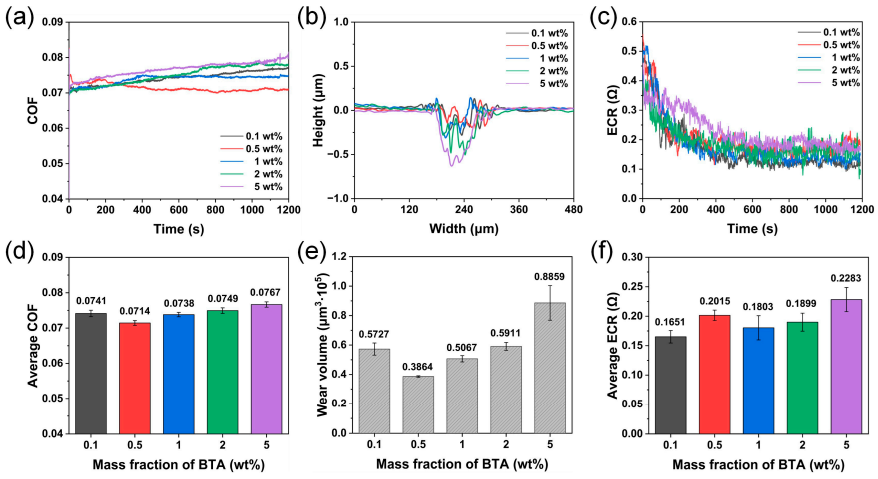

Figure 6. Tribological behavior of BTA with different mass fractions as an ionic liquid additive under a 0.5 A current: (**a**) coefficients of friction, (**b**) cross-sectional profile of the wear scars, (**c**) electrical contact resistances, (**d**) average coefficients of friction, (**e**) wear volumes, and (**f**) average electrical contact resistances.

The ECR curves and corresponding average ECR values under different BTA concentrations are shown in Figure 6c,f, respectively. In the 0.1–1 wt% concentration range, the ECR exhibited an inverse trend compared to the COF. However, at concentrations between 2 and 5 wt%, higher ECR was observed. The ECR can effectively indicate the presence and state of the lubricating film and the formation and degradation of the film over time [28]. However, studies have suggested that frictional wear and film formation are not necessarily linearly related [29]. A thicker surface film can create significant interfacial stress, making it more prone to mechanical removal and increasing material wear [30].

At high BTA concentrations, BTA is speculated to continuously react with fresh metal, forming an unstable reaction film at the friction interface. This reaction film forms repeatedly and peels off due to friction, negatively affecting the overall stability of the lubricating film and leading to increased wear. In addition, as the BTA reaction film is removed by friction, a continuous protective layer cannot form, limiting its ability to effectively inhibit IL-induced corrosion at the friction interface. Furthermore, the exposed fresh metal surface continually undergoes tribochemical reactions, generating more tribochemical reaction products at the friction interface. However, due to the inherent instability of the lubricating film, the non-conductive films formed by these tribochemical products at the friction interface fail to contribute significantly to reducing friction. Thus, the aforementioned reasons contribute to the increased wear volume and ECR observed under excessively high BTA concentrations in the IL. These results suggest that the effect of BTA as an IL additive is concentration-dependent, significantly influencing both frictional wear and ECR.

Figure 7 shows the three-dimensional morphologies and optical microscope images of wear scars obtained after friction with varying concentrations of BTA added to the IL lubricant. At a BTA concentration of 0.1 wt%, the wear scar exhibited a width of 167.52 µm and a depth of 0.3 µm. At a BTA concentration of 0.5 wt%, the wear scar width and depth decreased to 110.91 and 0.21 µm, respectively. However, when the BTA concentration exceeded 0.5 wt%, the cross-sectional dimensions of the wear scars increased with further increases in BTA concentration. At a BTA concentration of 5 wt%, the wear scar width was 30% larger than that at 0.5 wt%, and the wear depth doubled. These results indicate that the addition of BTA provides optimal performance at an appropriate concentration, whereas excessive concentrations can lead to severe wear. Under a 0.5 A applied current, the optimal lubrication performance was achieved at a BTA concentration of 0.5 wt%, and therefore, this concentration was selected for further research.

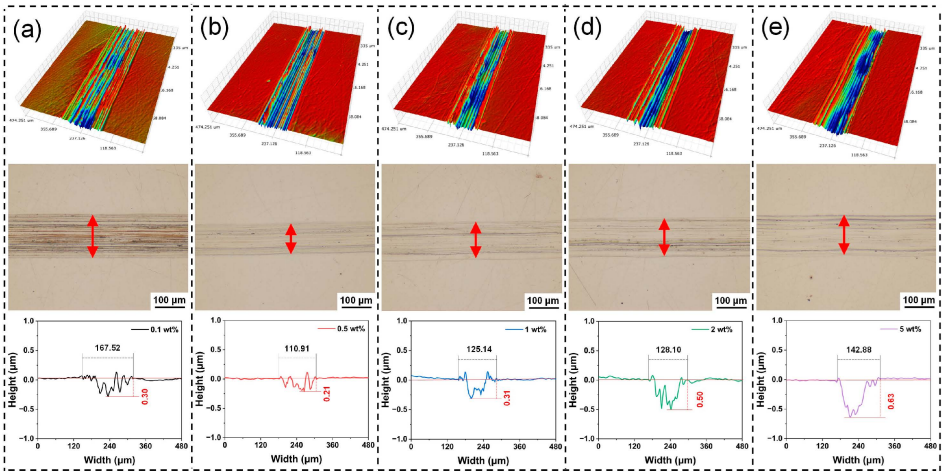

Figure 7. Surface morphologies of wear scars after friction under a 0.5 A current with IL lubrication at BTA mass fractions of (**a**) 0.1 wt%, (**b**) 0.5 wt%, (**c**) 1 wt%, (**d**) 2 wt%, and (**e**) 5 wt%.

3.2.3. Effect of Applied Current

The effects of applied current on the COF and ECR were investigated to evaluate the current-carrying capacity of BTA as an additive in the IL lubricant. As depicted in Figure 8a, the COF of the IL lubricant with 0.5 wt% BTA was greater than that of the IL lubricant without BTA at 0 A; however, the opposite results were observed when an external current was applied. Figure 8b shows that at a current of 0.5 A, the COF under 0.5 wt% BTA lubrication was lower than that under pure IL lubrication. To verify this change, we tested the COF and wear volume at different BTA concentrations under 0 A, with results included in Figure 8a. The results indicate that, at 0 A, a concentration of 0.1 wt% BTA provided excellent capability to reduce friction and wear, while concentrations of 0.5 wt% and above led to significant increases in both COF and wear volume. This implies that the current may affect the performance or action mechanism of BTA as an IL additive. Additionally, it was observed that under a low current of 0.5 A, the initial ECRs for both lubrication conditions were relatively high and stabilized after approximately 200 s. As the current increased, this phenomenon gradually disappeared. This reflects the influence of current intensity on the lubrication state, where higher currents promote the formation of a stable lubrication state within a shorter time frame.

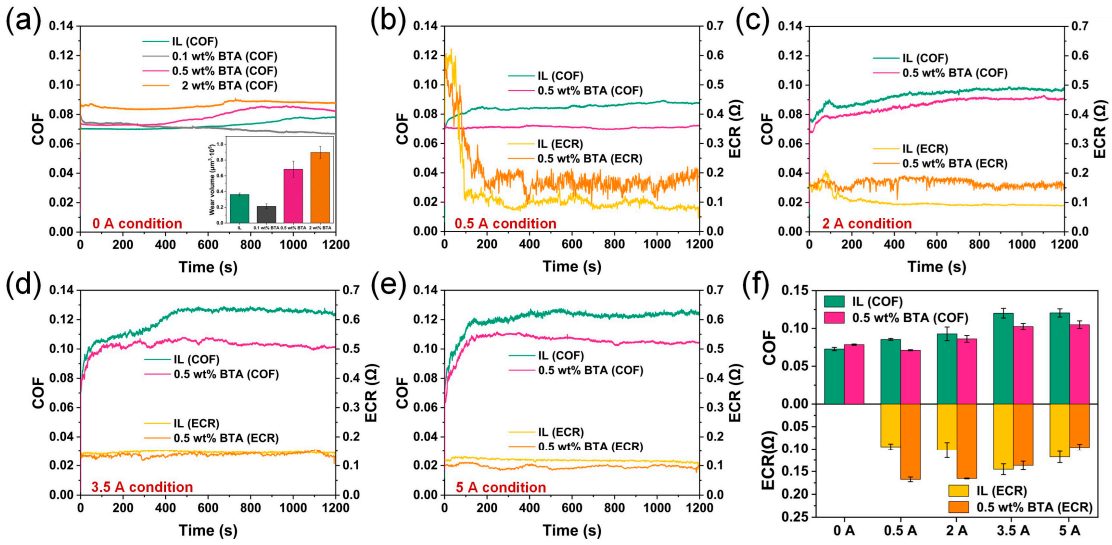

Figure 8. Tribological behaviors of steel ball–plate pairs under pure IL and 0.5 wt% BTA lubrication at current loads of (**a**) 0 A, (**b**) 0.5 A, (**c**) 2 A, (**d**) 3.5 A, and (**e**) 5 A. (**f**) Average coefficient of friction and electrical contact resistance in each case.

The COF and ECR at a current of 2 A are shown in Figure 8c, where the results are consistent with those obtained at 0.5 A: the COF under 0.5 wt% BTA lubrication was lower than that under pure IL lubrication, whereas the ECR was relatively higher. As shown in Figure 8d, at a current of 3.5 A, a significant change in ECR was observed between the two lubrication conditions. Under a 0.5 wt% BTA lubrication, the ECR was nearly the same as that under pure IL lubrication. The test results at a current of 5 A are shown in Figure 8e, which indicate that the COF and ECR under 0.5 wt% BTA lubrication were relatively low.

Figure 8f compares the average COF and stabilized ECR values under IL and 0.5 wt% BTA lubrication across a current range from 0 to 5 A. Under pure IL lubrication, both the COF and ECR showed an increasing trend with an increase in current. The COF of the IL increased when the current increased from 0 to 0.5 A. As the current gradually increased to 5 A, the continuous intensification of arc erosion effects led to a worsening frictional state, thereby causing a sustained increase in the COF. In contrast, under 0.5 wt% BTA lubrication, the COF decreased when the current increased from 0 A to 0.5 A, and then, it continued to

rise with further increases in current. The COFs under 0.5 wt% BTA lubrication across the 0.5–5 A current range were consistently lower than those under IL lubrication. Additionally, the ECR showed a decreasing trend as the current increased.

Figure 9 compares the wear scar morphologies of steel balls under different applied currents using an optical microscope. Under pure ionic liquid lubrication, the diameter of the steel ball wear scars increased progressively with the applied current. At 0 A, the addition of 0.5 wt% BTA led to an increase in the wear scar diameter. In contrast, within the range of 0.5–5 A, the wear scar diameters under 0.5 wt% BTA lubrication were consistently smaller than those under pure ionic liquid lubrication. The variation in wear scar diameter corresponds to the COF trends under different applied currents shown in Figure 8. Within the 0.5–5 A current range, the addition of BTA resulted in visibly smoother wear scar surfaces and lighter coloration, suggesting its potential to suppress friction-induced corrosion under current-carrying friction conditions.

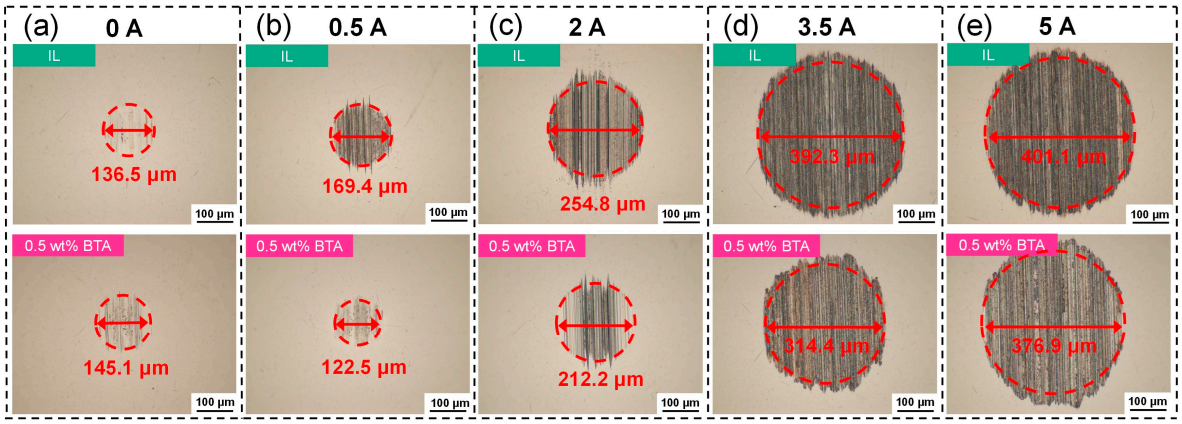

Figure 9. Optical micrographs of wear scars on steel balls under different current loads with BTA as an ionic liquid additive: (**a**) 0 A, (**b**) 0.5 A, (**c**) 2 A, (**d**) 3.5 A, and (**e**) 5 A.

Figure 10 provides an intuitive comparison of wear scar morphologies on steel plates obtained under different applied currents using an optical microscope and a 3D white-light interferometer. By comparing the wear morphologies of steel balls and steel plates under varying applied currents, it is observed that the trend in wear scar diameter on the steel balls corresponds closely to the trend in wear scar width on the steel plates. Figure 10a compares the wear scar morphologies at a 0 A current. Although the wear scar surface under 0.5 wt% BTA lubrication appeared smoother, the cross-sectional profiles indicate that adding 0.5 wt% BTA at 0 A increased wear. It is noteworthy that the opposite result was observed at 0.5 A. As shown in Figure 10b, the wear was relatively smaller under 0.5 wt% BTA lubrication. Figure 10c shows that the wear volumes under both lubrication conditions increased notably when the current increased to 2 A, with the intensified arc erosion leading to a darker color on the wear scar surface. Figure 10d reveals that a noticeable change in wear type occurred as the current increased to 3.5 A, with adhesive wear characteristics clearly observable in the optical microscope images. Comparing the cross-sectional profiles at this current revealed that the wear scar width and extent of adhesive wear under 0.5 wt% BTA lubrication were smaller than those under IL lubrication. As shown in Figure 10e, the wear scar morphology exhibited more severe adhesive wear when the current was further increased to 5 A. Even so, adding BTA to the IL lubricant still effectively reduced the wear severity. These findings indicate that under current-carrying friction conditions, an appropriate concentration of BTA can effectively reduce wear on both frictional surfaces of the ball–plate pair.

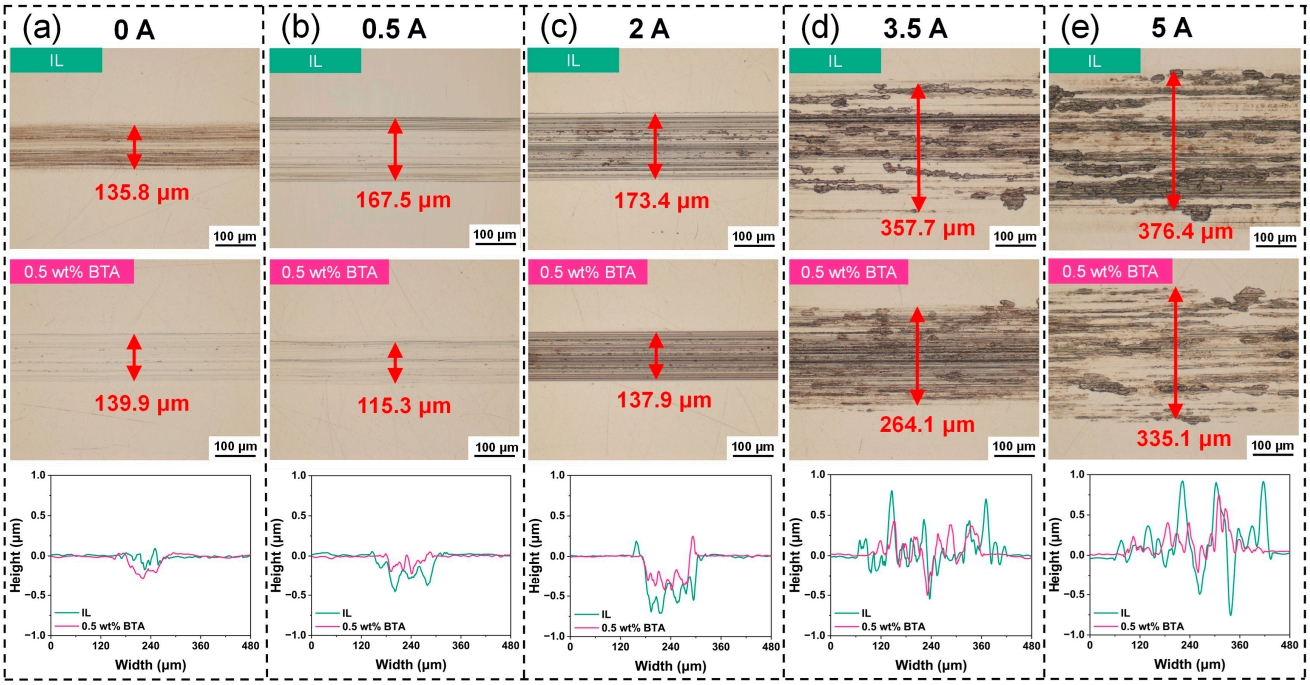

Figure 10. Optical micrographs and cross-sectional profiles of wear scars on steel plates under different current loads with BTA as an ionic liquid additive: (**a**) 0 A, (**b**) 0.5 A, (**c**) 2 A, (**d**) 3.5 A, and (**e**) 5 A.

3.3. Analysis of Worn Surface

3.3.1. Surface Morphologies

Figure 11 compares the SEM images of the worn steel plate surfaces to further investigate the effect of BTA on IL lubrication performance under different applied currents. Figure 11a shows the wear scar morphologies obtained under IL lubrication and 0.5 wt% BTA lubrication at a current of 0 A. Both conditions exhibited typical abrasive wear characteristics; however, the width and depth of the wear grooves were greater under 0.5 wt% BTA lubrication. The results in Figure 8a confirm that 0.5 wt% is not the optimal concentration under 0 A conditions because high BTA concentrations increase wear. As depicted in Figure 11b, when a current of 0.5 A was applied, the degree of abrasive wear increased under pure IL lubrication, with more pronounced wear grooves; however, the wear surface under 0.5 wt% BTA lubrication was smoother. This indicated that wear increased with IL lubrication after current application, whereas it decreased under 0.5 wt% BTA lubrication. Figure 11c shows that both lubrication conditions exhibited typical abrasive wear characteristics with significantly increased wear when a current of 2 A was applied. Distinct pitting was observed on the wear surface under pure IL lubrication, likely because of the combined effects of IL corrosion and electrical erosion. In contrast, no significant pitting was observed on the wear surface under 0.5 wt% BTA lubrication. Figure 11d,e show that, the wear scar morphologies under both lubrication conditions exhibited mixed characteristics of abrasive and adhesive wear as the current load increased to 3.5 A and above, with large spalling pits on the wear surface caused by intensified electrical erosion. Comparatively, the 0.5 wt% BTA lubrication condition showed fewer spalling pits and a lower degree of adhesive wear. Therefore, the SEM analysis results indicate that adding BTA to the IL lubricant can effectively reduce frictional wear and mitigate arc erosion damage to friction pair surfaces.

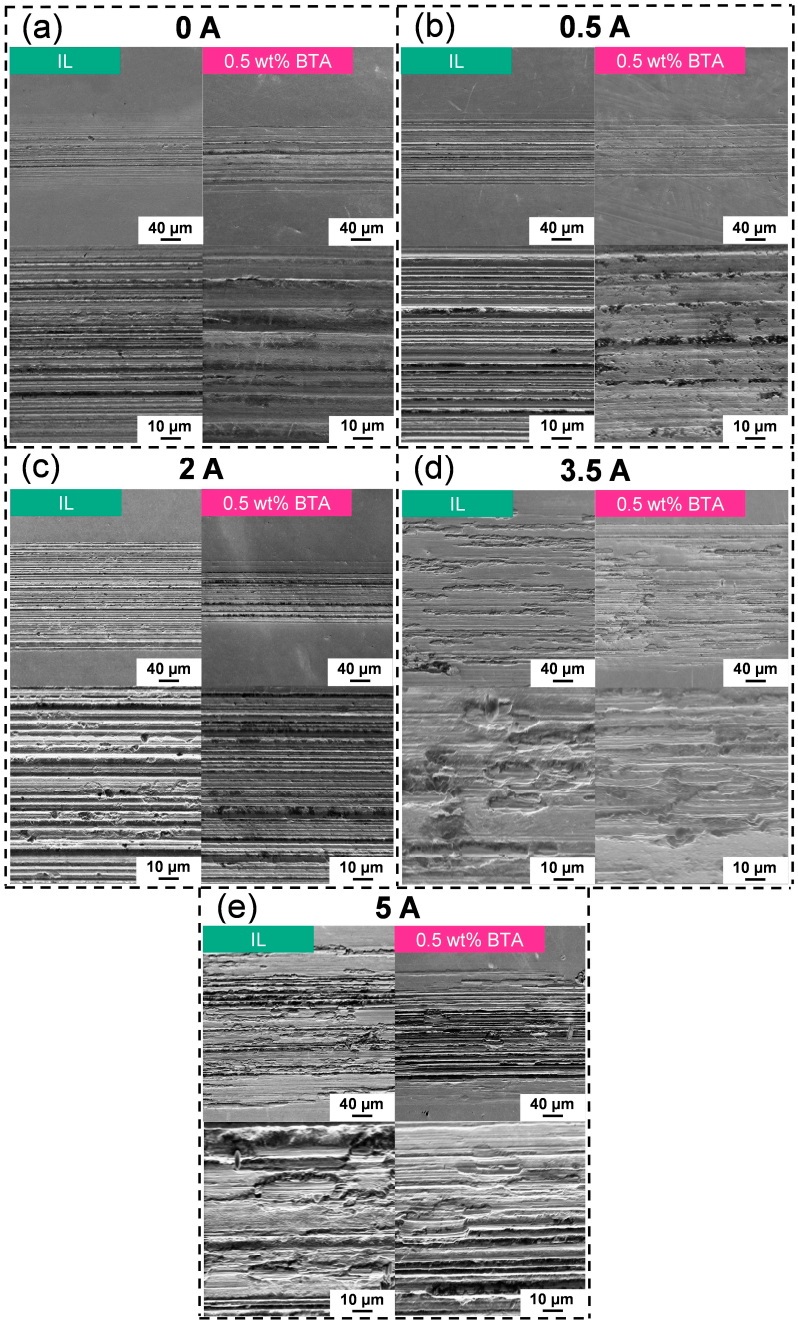

Figure 11. SEM images of steel plate surfaces after friction using 0.5 wt% BTA added to IL lubricant at applied currents of (**a**) 0 A, (**b**) 0.5 A, (**c**) 2 A, (**d**) 3.5 A, and (**e**) 5 A.

3.3.2. Surface Compositions

EDS mapping was used to analyze the worn surfaces and determine the relative contents of carbon, iron, oxygen, fluorine, and nitrogen elements, as shown in Table 2. Because of the low N content, its relative percentage was nearly negligible. At currents of 0, 0.5, and 2 A, the relative O contents on the wear scar surfaces were higher under 0.5 wt% BTA lubrication than under pure IL lubrication; however, the O contents under the two lubrication conditions were similar at a 3.5 A current. At a 5 A current, the O content was lower under 0.5% BTA lubrication than that under pure IL lubrication. The relative O contents on the worn surfaces were closely correlated with the ECR measurements obtained during the current-carrying friction tests: a higher O content corresponded to an increased ECR because the oxides present at a friction interface formed non-conductive films that increased in resistance with an increase in their content. Therefore, this phenomenon

reflected the insulating effect of oxide films formed at the electrical contact interface, affecting the overall electrical performance.

Table 2. EDS analysis of worn surface elements under different experimental conditions.

Experimental Condition		C (%)	O (%)	Fe (%)	F (%)	N (%)
0 A	IL	84.2	2.3	13.0	0.5	0.0
	0.5 wt% BTA	82.4	4.1	12.9	0.6	0.0
0.5 A	IL	84.8	2.4	12.8	0.0	0.0
	0.5 wt% BTA	84.6	4.7	10.7	0.0	0.0
2 A	IL	83.8	2.1	13.9	0.2	0.0
	0.5 wt% BTA	84.5	4.1	11.3	0.0	0.0
3.5 A	IL	80.4	3.0	16.6	0.0	0.0
	0.5 wt% BTA	84.9	3.0	11.9	0.2	0.0
5 A	IL	82.4	3.0	14.4	0.2	0.0
	0.5 wt% BTA	81.2	1.7	17.1	0.0	0.0

XPS was used to compare and analyze the elemental compositions and relative content of the worn surfaces under IL and 0.5 wt% BTA lubrication at different applied currents. Figure 12 illustrates the chemical states of the worn surfaces under lubrication with two different lubricants at 0 A. The fitted peaks of the C 1s spectrum were located at ~284.80 eV (C–C/C–H), 286.48 eV (C–N), and 288.40 eV (C=O) [31]. Three representative peaks were identified in the O 1s spectrum at ~529.68 eV (Fe–O), 531.37 eV (C=O), and 532.90 eV (N–O) [32]. The Fe 2p spectrum exhibited a peak at ~706.76 eV, indicating the presence of elemental iron; the peaks observed at ~710.46 and 723.96 eV correspond to Fe^{2+} oxides in the $2p_{3/2}$ and $2p_{1/2}$ orbitals, respectively; the peaks at ~713.74 and 727.77 eV correspond to Fe^{3+} oxides in the $2p_{3/2}$ and $2p_{1/2}$ orbitals, respectively; and the peak at ~719.27 eV represents a satellite peak of Fe [33,34]. These results suggest that tribochemical reactions occurred during the friction process, with the corresponding products possibly including iron oxides such as FeO, Fe_2O_3, FeOOH, and Fe_3O_4. The characteristic peak of F 1s appeared near 683.98 eV. When combined with the Fe 2p spectrum analysis, F from the IL participated in the tribochemical reactions, resulting in the formation of metal fluorides, such as iron fluoride (FeF_3) or ferrous fluoride (FeF_2), on the friction surface [35]. The fitted peak of N 1s detected at ~399.91 eV is attributed to carbon nitrides or nitrogen oxides [25]. A quantitative analysis of the relative contents of the products in the O 1s and Fe 2p spectra at 0 A was undertaken by measuring the XPS peak areas; the results in Table 3 indicate that the relative contents of Fe–O and Fe^{3+} oxides were higher under 0.5 wt% BTA lubrication than that under IL lubrication.

Table 3. Proportions of components in the O 1s and Fe 2p spectra at an applied current of 0 A.

Lubricant	Component (O)	Proportion (%)	Component (Fe)	Proportion (%)
IL	Fe–O	40.56	Fe	7.08
	C=O	51.72	$Fe^{2+}{}_xO_y$	70.25
	N–O	7.72	$Fe^{3+}{}_mO_n$	22.67
0.5 wt% BTA	Fe–O	55.90	Fe	6.31
	C=O	31.82	$Fe^{2+}{}_xO_y$	68.50
	N–O	12.28	$Fe^{3+}{}_mO_n$	25.19

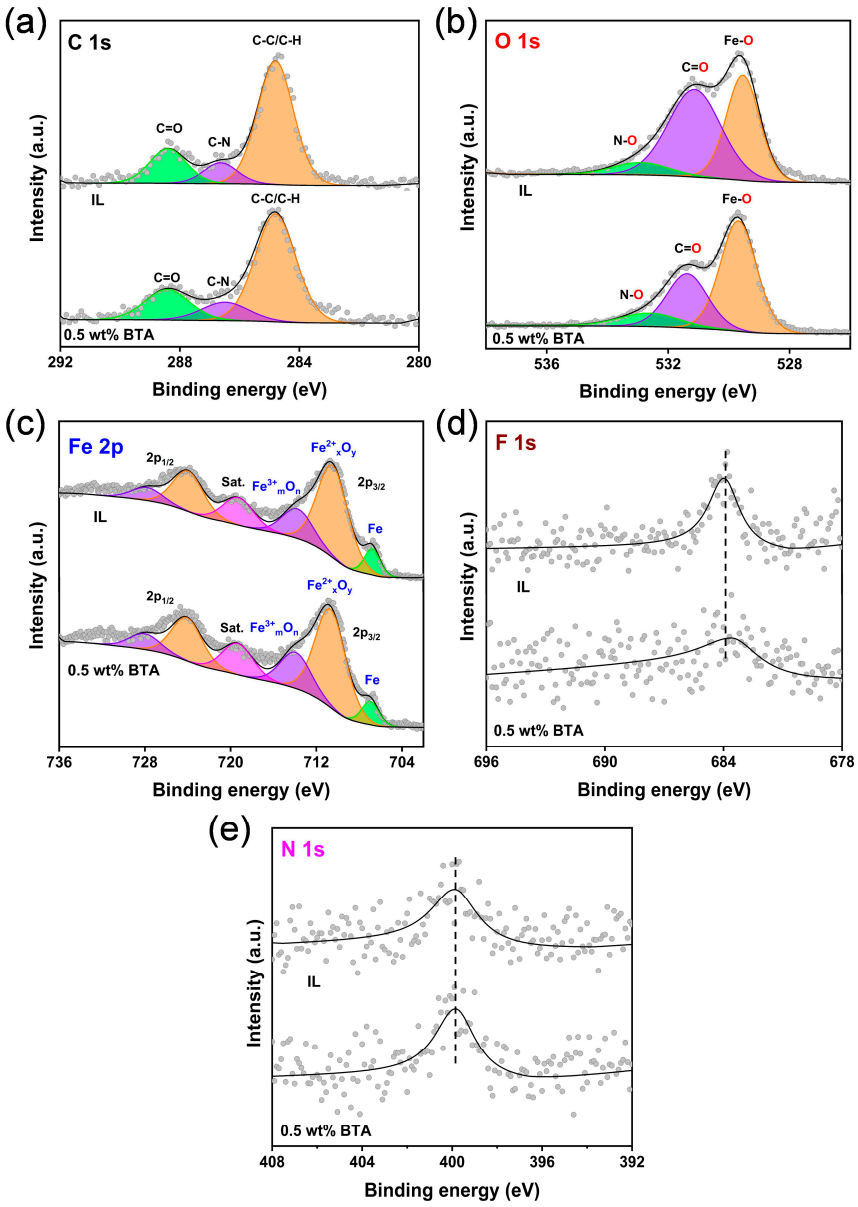

Figure 12. XPS spectra of worn surfaces lubricated with pure IL and 0.5 wt% BTA at an applied current of 0 A: (**a**) C 1s Spectrum, (**b**) O 1s Spectrum, (**c**) Fe 2p Spectrum, (**d**) F 1s Spectrum, and (**e**) N 1s Spectrum.

The XPS results for the worn surfaces obtained after friction at a low current of 0.5 A are shown in Figure 13. Peaks in the C 1s spectrum were observed at ~284.80 eV, 286.42 eV, and 288.26 eV, while the O 1s spectrum displayed peaks at ~529.78 eV, 531.50 eV, and 533.41 eV. The Fe 2p spectrum exhibited peaks at ~706.37 eV, 709.85 eV, and 712.65 eV. The F 1s spectrum showed a peak at ~684.01 eV, while the N 1s spectrum displayed a peak at ~399.85 eV, consistent with the peaks observed in Figure 12. The relative contents of the products in the O 1s and Fe 2p spectra at a low current of 0.5 A were quantitatively analyzed by calculating the peak areas, with the results presented in Table 4. Compared to IL lubrication, the relative contents of Fe–O and Fe^{3+} oxides were higher under 0.5 wt% BTA lubrication, indicating that using BTA as an additive in IL promoted oxidation reactions at a low current, as seen at 0 A. It is noteworthy that, compared to the 0 A condition, the metal oxide content is reduced under the 0.5 A low current with 0.5 wt% BTA lubrication.

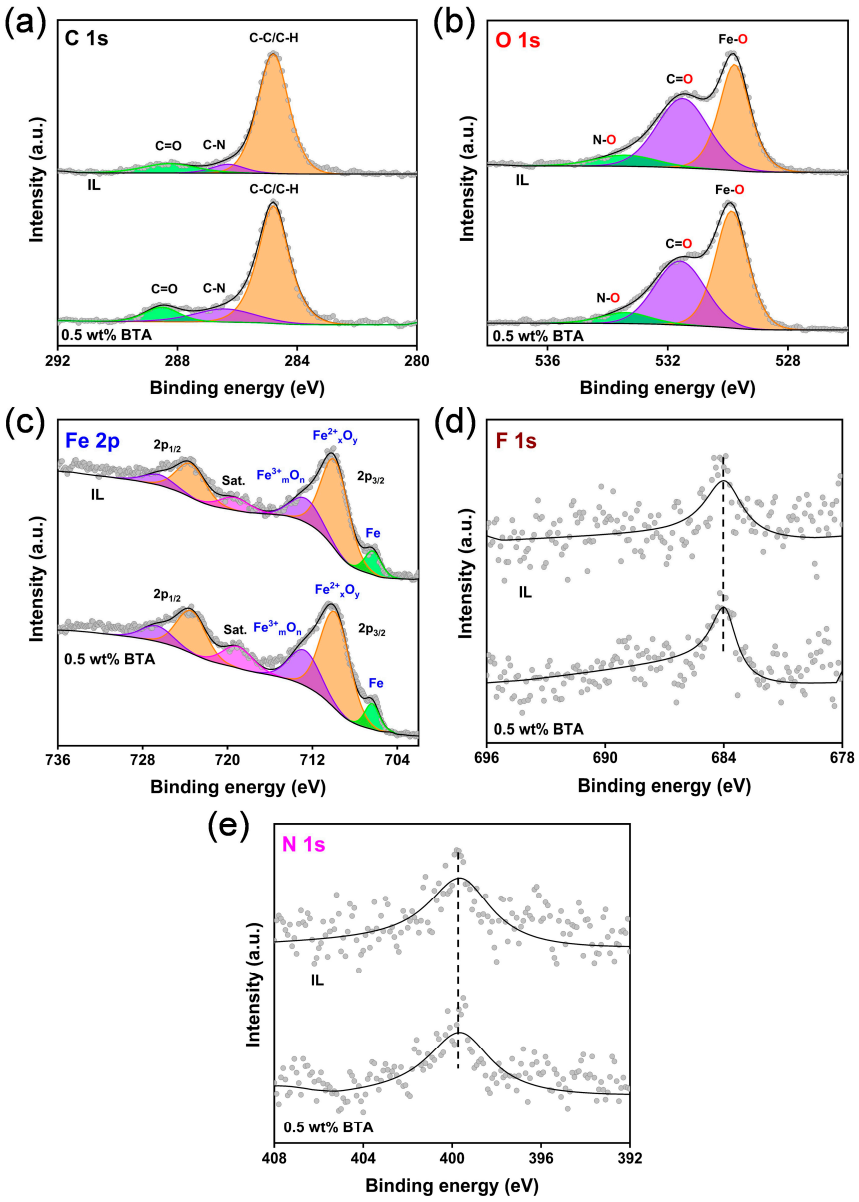

Figure 13. XPS spectra of worn surfaces lubricated with pure IL and 0.5 wt% BTA at an applied current of 0.5 A: (**a**) C 1s Spectrum, (**b**) O 1s Spectrum, (**c**) Fe 2p Spectrum, (**d**) F 1s Spectrum, and (**e**) N 1s Spectrum.

Table 4. Proportions of components in the O 1s and Fe 2p spectra at an applied current of 0.5 A.

Lubricant	Component (O)	Proportion (%)	Component (Fe)	Proportion (%)
IL	Fe–O	44.43	Fe	7.87
	C=O	46.69	$Fe^{2+}{}_xO_y$	70.88
	N–O	8.88	$Fe^{3+}{}_mO_n$	21.25
0.5 wt% BTA	Fe–O	51.41	Fe	6.29
	C=O	41.38	$Fe^{2+}{}_xO_y$	67.73
	N–O	7.21	$Fe^{3+}{}_mO_n$	25.98

The XPS results for the worn surfaces at a high current of 5 A are presented in Figure 14. Peaks were observed in the C 1s spectrum at ~284.80 eV, 286.83 eV, and 288.40 eV, while the O 1s spectrum displayed peaks at ~529.52 eV, 531.42 eV, and 533.17 eV. The Fe 2p spectrum displayed peaks at ~706.48 eV, 710.34 eV, and 713.32 eV, while the N 1s spectrum showed a peak at ~399.73 eV, consistent with the peaks observed in Figure 12. The F 1s spectrum

shows a C–F peak near 688.76 eV, indicating the presence of organofluorine on the worn surface, suggesting that high current may have facilitated the occurrence of the relevant chemical reactions [36]. The relative contents of the products in the O 1s and Fe 2p spectra at a current of 5 A were quantitatively analyzed by calculating peak areas with the results presented in Table 5. At a high current of 5 A, the addition of BTA to the IL lubricant further reduced the content of metal oxides on the friction surface.

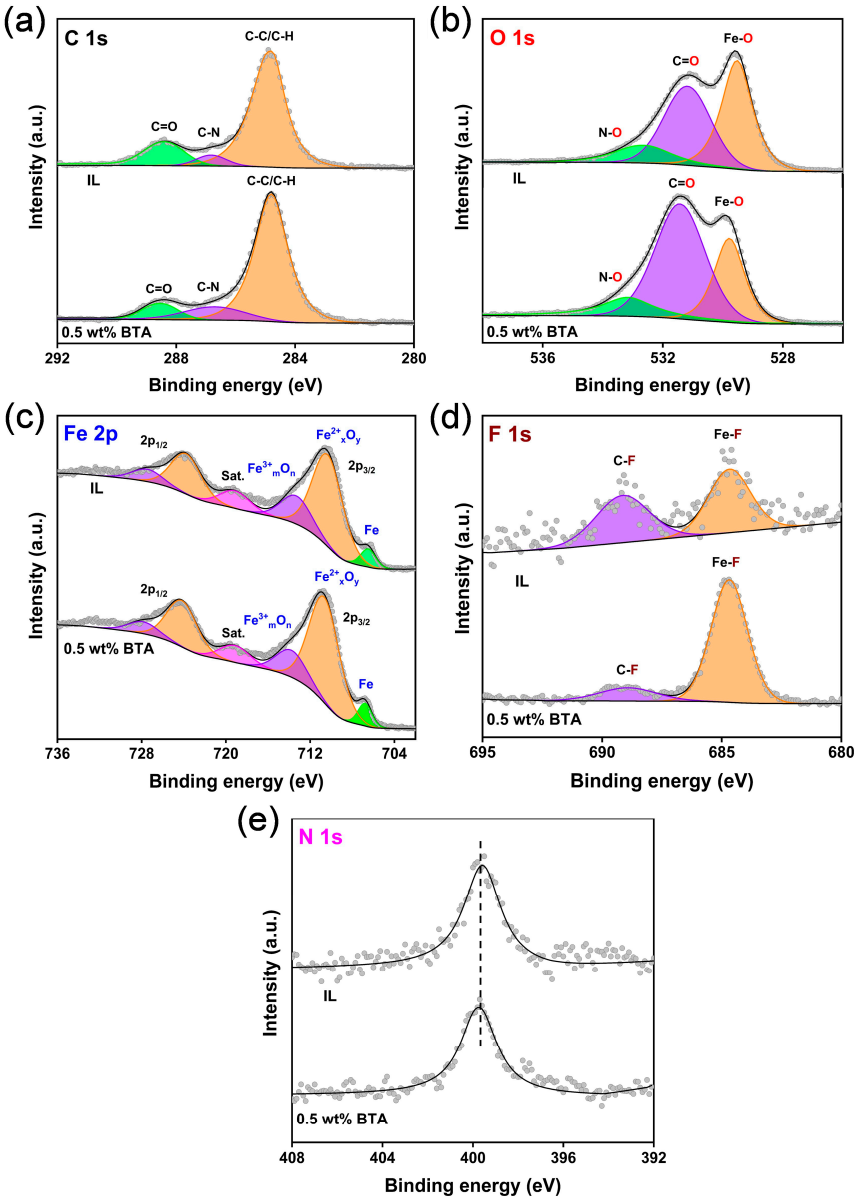

Figure 14. XPS spectra of worn surfaces lubricated with pure IL and 0.5 wt% BTA at an applied current of 5 A: (**a**) C 1s Spectrum, (**b**) O 1s Spectrum, (**c**) Fe 2p Spectrum, (**d**) F 1s Spectrum, and (**e**) N 1s Spectrum.

In summary, the elemental analysis of the worn surfaces indicates that the variation trend of the relative content of metal oxides observed in the XPS analysis is consistent with the trend of the relative oxygen content observed in the EDS analysis under different applied currents. Under IL lubrication, the oxide content on the worn surface increased with rising current; in contrast, under 0.5 wt% BTA lubrication, the oxide content decreased as the current increased. These results suggest that the presence of BTA may inhibit oxidation reactions during the friction process as the current increases.

Table 5. Proportions of components in the O 1s and Fe 2p spectra at an applied current of 5 A.

Lubricant	Component (O)	Proportion (%)	Component (Fe)	Proportion (%)
IL	Fe–O	43.48	Fe	4.99
	C=O	43.73	$Fe^{2+}{}_xO_y$	72.67
	N–O	12.79	$Fe^{3+}{}_mO_n$	22.34
0.5 wt% BTA	Fe–O	27.65	Fe	5.13
	C=O	59.07	$Fe^{2+}{}_xO_y$	75.56
	N–O	13.28	$Fe^{3+}{}_mO_n$	19.31

3.3.3. Raman Spectroscopic Analysis

Raman spectroscopy was employed to analyze the worn surfaces, offering insights into their chemical composition and molecular structure. The Raman spectra of worn surfaces under dry friction, pure IL lubrication, and 0.5 wt% BTA lubrication are shown in Figure 15a–c, respectively. The peaks at 602 cm^{-1}, 661 cm^{-1}, and 683 cm^{-1} are characteristic of tribochemical reactions occurring under all three lubrication conditions, resulting in the formation of iron oxides like FeO and Fe_3O_4 [37].

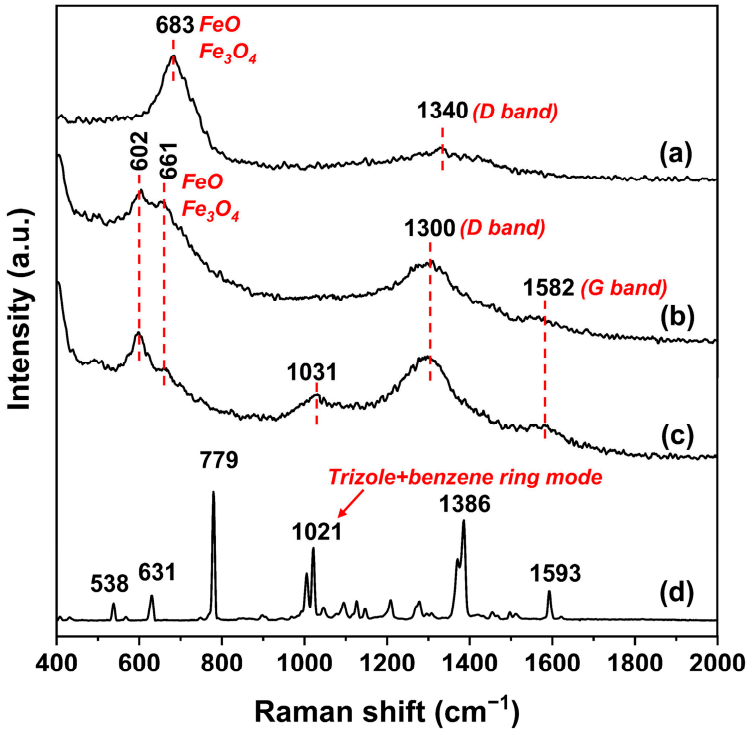

Figure 15. Raman spectra of wear surfaces under different lubrication conditions and solid BTA: (**a**) dry friction, (**b**) pure IL lubrication, (**c**) 0.5 wt% BTA lubrication at 0.5 A applied current, and (**d**) solid BTA.

Under dry friction conditions, a D band was observed at 1340 cm^{-1}, with no G band detected, indicating significant structural defects on the worn surface. Intense shear forces and localized high temperatures disrupted the ordered structure of carbon materials on the worn surface, leading to the formation of numerous defects and disordered carbon structures. In contrast, the G band detected on the worn surfaces under pure IL and 0.5 wt% BTA lubrication suggests that the lubricants effectively reduced friction and wear, thereby minimizing carbon molecular defects on the worn surface. In addition, the shift in the D band from 1340 cm^{-1} to 1300 cm^{-1} also partially reflects the protective effect of the lubricant on the friction surface [38].

Figure 15d displays the Raman spectrum of solid BTA, where the peak at 1021 cm^{-1} represents the synergistic vibration of the benzene and triazole rings in the BTA molecule [39]. Previous studies have demonstrated that after coordination with different metals, the peak at 1021 cm^{-1} shifts to higher wavenumbers, with the magnitude of the shift depending on the type of metal. As shown in Figure 15c, the peak at 1021 cm^{-1} shifted to 1031 cm^{-1}, which is often used as direct evidence for the coordination structure of BTA on metal surfaces. This observation indicates the presence of BTA-Fe complexes on the worn surfaces under 0.5 wt% BTA lubrication [40,41].

3.4. Mechanism Analysis

The tribological test and worn surface characterization results were analyzed to infer the possible lubrication mechanisms occurring during the friction process. Under IL lubrication conditions, the COF, wear volume, and ECR exhibited an increasing trend with the applied current. Studies have shown that ILs containing $PF6^-$ anions can cause severe corrosion because of the hydrolysis of fluorine-containing anions during friction, which leads to the formation of highly corrosive HF acid, impairing anti-friction and anti-wear properties [19,20]. Increasing current intensifies tribochemical reactions as the localized temperature at the friction surface rises because of Joule heating, which can promote $PF6^-$ hydrolysis, exacerbating corrosion and wear under electric current. In addition, the arc erosion effect cannot be ignored. Micro gaps at the friction interface trigger arcs that lead to localized high temperatures and electrical ablation, further damaging the friction surface. Arc erosion not only promotes oxidative wear of the contact metal surfaces but can also compromise the integrity of the lubricating film, resulting in a significant decline in lubrication performance [42]. The SEM analysis reveals that, with continuous increases in current, the degree of wear progressively worsens, transitioning from abrasive wear to adhesive wear. This change occurs because intensified arc erosion raises the localized temperature at the electrical contact surface, causing material softening and increasing adhesion between metal surfaces [31]. Therefore, we conclude that the corrosiveness of ILs and the arc erosion effect are the primary factors causing increased friction and wear with increasing current. The elemental analysis results indicate that the relative content of oxides on the friction surface increased with current, suggesting that the elevated current accelerates oxidation reactions during the friction process. The oxides form a non-conductive film over the friction surface, consequently increasing ECR [43].

The lone pair of electrons of nitrogen atoms in BTA can coordinate with Fe to form stable metal complexes [44–46]. Previous studies have shown that the coordination reaction film formed between BTA and metals exhibits excellent lubricating performance, which is only achievable at an appropriate additive concentration [23]. Further, the results of this study support this finding. Under no current, adding 0.5 wt% BTA to IL increased friction and wear, as 0.5 wt% is considered a high concentration at 0 A, whereas 0.1 wt% BTA could achieve effective friction reduction. In addition, we compared the current-carrying tribological performance at 0.5 A with different BTA concentrations. The results indicated that, at 0.5 wt% under 0.5 A, the COF and wear volume were minimized, suggesting that current can influence the effect and action mechanism of BTA. When the concentration of BTA is within the optimal range under specific conditions, a steady downward trend in the COF curve is observed. This may be attributed to an appropriate amount of BTA reacting with the metal surface during the friction process to form a stable lubrication film, thereby reducing direct contact and improving the lubrication state. As the reaction film gradually stabilizes, the anti-friction and anti-wear performance of the friction interface is enhanced.

High concentrations of BTA increase the COF, wear volume, and ECR. This is because excess BTA continuously reacts with fresh metal, forming an unstable BTA-Fe reaction film

that repeatedly forms and peels off during friction, leading to increased wear. Meanwhile, the newly exposed metal not only undergoes further complexation with BTA but also continuously participates in tribochemical reactions, increasing the amount of oxidation products and, consequently, ECR. The elemental analysis results of the worn surface support this observation: at 0 A, the relative content of oxides on the worn surface under 0.5 wt% BTA lubrication is higher. In contrast, under the same lubrication condition, the relative content of oxides decreases when a 0.5 A current is applied.

The results of electrochemical corrosion tests show that in the corrosive environment of IL, BTA at a concentration of 1 wt% exhibits the best corrosion inhibition performance, with the corrosion current density and corrosion rate reduced by two orders of magnitude compared to pure IL. Combined with the results of tribological tests, it is evident that adding low concentrations of BTA to the IL can effectively achieve both corrosion inhibition and lubrication. Specifically, 1 wt% BTA demonstrates the best corrosion inhibition capacity, while 0.5 wt% BTA shows optimal lubricating performance. In addition, the electrochemical corrosion test results further support the potential and effectiveness of low-concentration BTA in mitigating tribocorrosion.

Studies have shown that ILs can form electrically enhanced adsorption layers at friction interfaces under electric fields, with greater ionic adsorption at higher currents, resulting in better lubricating performance than that of ILs without current [47]. We speculate that the electrically enhanced IL adsorption layer under an electric field suppresses the frictional removal of the BTA-Fe reaction film, improving the stability of the lubricating film. When the current increases to 5 A, the relative oxide content on the worn surface under 0.5 wt% BTA lubrication further decreases. This is because, as the current increases, the adsorption capability of the electrically enhanced IL adsorption layer at the interface is further strengthened, further inhibiting the frictional removal of the BTA-Fe reaction film. A denser BTA-Fe reaction film at the friction interface not only effectively prevents IL-induced corrosion at the friction interface and reduces arc erosion damage to the friction surface but also inhibits oxidation reactions during friction. We believe that the coupled effects of the BTA-Fe reaction film and the electrically enhanced IL adsorption layer under current-carrying friction conditions improve the overall performance of the lubricating film. SEM analysis shows that, within the current range of 0.5–5 A, an appropriate concentration of BTA as an IL additive effectively reduces wear and arc erosion damage to the friction surface, demonstrating superior friction-reducing and anti-wear performance.

Based on the above analysis, we conclude that BTA and IL lubricants exhibit a synergistic effect in enhancing lubrication and corrosion resistance under current-carrying friction conditions. On the one hand, the electrically enhanced adsorption layer of IL suppresses the frictional removal of the BTA-Fe reaction film, improving the stability of the lubricating film. On the other hand, the BTA-Fe reaction film not only effectively reduces arc erosion damage to the friction surface but also inhibits IL-induced corrosion at the friction interface through its physical isolation effect. The presence of the BTA-Fe reaction film at the friction interface, combined with the electrically enhanced adsorption behavior of IL at the interface, is the primary reason for the improved performance of the lubricant. When added to IL as a corrosion inhibitor, BTA demonstrates different wear and lubrication mechanisms under varying current loads, as illustrated in Figure 16.

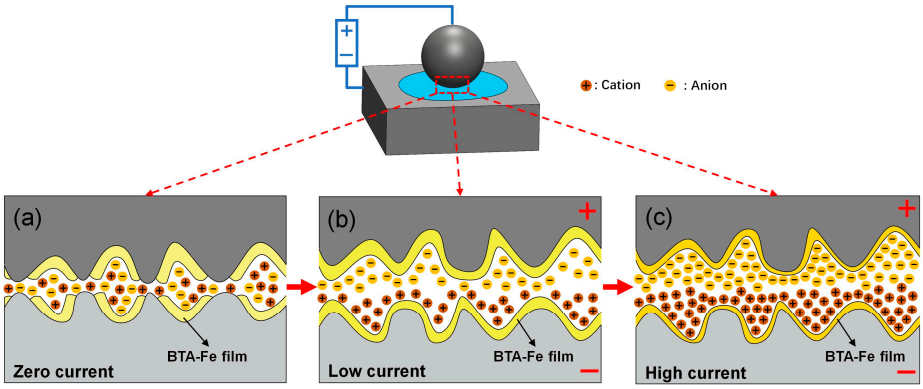

Figure 16. Schematic of the wear mechanisms when using BTA added to an IL lubricant: (**a**) zero current (0 A), (**b**) low current (0.5 A), and (**c**) high current (5 A).

4. Conclusions

The continuous development of the electrical industry has driven extensive research and application of conductive lubricants in tribology. However, the issue of corrosive wear associated with ILs as conductive lubricants limits their practical application. This study systematically evaluated the effects of adding BTA to the IL lubricant at different concentrations and applied currents, aiming to reveal the synergistic mechanisms between BTA and IL. The experimental results show that the performance of BTA is concentration-dependent: an appropriate concentration optimizes the lubricating performance of IL, while an excessive concentration negatively impacts its anti-wear and lubricating properties. At a current of 0.5 A, the IL lubricant with 0.5 wt% BTA demonstrated optimal performance, reducing the COF and wear volume by 16.5% and 53.4%, respectively, compared to pure IL lubrication. Moreover, within the 0.5–5 A current range, an appropriate amount of BTA significantly enhanced the lubricating performance of IL, effectively suppressed its corrosive properties, and mitigated arc erosion damage on the friction surface. Wear scar characterization further revealed that the BTA-Fe reaction film reduced oxide formation on the worn surface under high currents, thereby lowering the ECR. In practical applications, such as conductive lubricants for electrical connectors, sliding switches, and bearings, BTA is recommended as an additive with an initial concentration range of 0.5–1.0 wt%. This relatively low concentration can achieve a balance between anti-wear protection and stable lubrication performance; however, its specific effectiveness still requires validation through practical application. This study underscores the synergistic lubrication and anti-corrosion effects of BTA and IL under current-carrying friction conditions. The findings offer valuable theoretical insights and practical strategies for advancing the application of IL as a high-performance conductive lubricant in engineering.

Author Contributions: Conceptualization, T.S. and M.Z.; methodology, K.P. and D.Z.; validation, L.S., Y.C. and Y.Y.; formal analysis, T.S. and L.S.; investigation, T.S.; resources, M.Z. and K.P.; data curation, T.S. and Y.C.; writing—original draft preparation, T.S.; writing—review and editing, M.Z.; visualization, D.Z.; supervision, M.Z.; project administration, M.Z. and K.P.; funding acquisition, M.Z. All authors have read and agreed to the published version of the manuscript.

Funding: This research was funded by the National Natural Science Foundation of China (Grant Number 12062002); the Guangxi Natural Science Foundation, China (Grant Number 2022GXNSFFA035036); the Guangxi Key Research and Development Plan, China (Grant Number AB23075091); the Guangxi Key Research and Development Plan, China (Grant Number AB24010035).

Data Availability Statement: The data presented in this study are available from the corresponding author upon reasonable request.

Conflicts of Interest: Author Taiyu Su and Ming Zhou were employed by the company Guangxi Tsinglube New Material Technology Co., Ltd. Author Kun Peng was employed by the company Guangxi Jianxing Guangyin New Material Technology Co., Ltd. The remaining authors declare that the research was conducted in the absence of any commercial or financial relationships that could be construed as a potential conflict of interest.

References

1. He, F.; Xie, G.; Luo, J. Electrical Bearing Failures in Electric Vehicles. *Friction* **2020**, *8*, 4–28. [CrossRef]
2. He, W.; Feng, Y.; Wu, S.; Wu, K.; Ye, J.; Wang, W. Numerical Simulation on the Effect of Current Intensity on Electrical Contact Performance of Electrical Connectors Subject to Micro-Slip Wear. *Wear* **2024**, *542–543*, 205270. [CrossRef]
3. Azevedo, C.R.F.; Sinatora, A. Failure Analysis of a Railway Copper Contact Strip. *Eng. Fail. Anal.* **2004**, *11*, 829–841. [CrossRef]
4. Noguchi, S.; Fukuda, E.; Kanada, T. Effect of Oil Film Parameter on Vibration Acceleration and Electrical Pitting of Small Ball Bearing. *Tribol. Online* **2012**, *7*, 33–40. [CrossRef]
5. Liu, X.; Zhou, C.; Zhou, X.; Hu, M.; Wang, D.; Xiao, Q.; Guan, X.; Zhang, W.; Zhang, S.; Xu, Z. Influence of different arc erosion durations on the wear properties of carbon skateboards/contact wires under low temperature. *Wear* **2023**, *516–517*, 204600. [CrossRef]
6. Grandin, M.; Wiklund, U. Wear Phenomena and Tribofilm Formation of Copper/Copper-Graphite Sliding Electrical Contact Materials. *Wear* **2018**, *398–399*, 227–235. [CrossRef]
7. Liu, X.; Cai, Z.; Xiao, Q.; Shen, M.; Yang, W.; Chen, D. Fretting Wear Behavior of Brass/Copper-Graphite Composites as a Contactor Material under Electrical Contact. *Int. J. Mech. Sci.* **2020**, *184*, 105703. [CrossRef]
8. Gao, J.; Zhou, M.; Cheng, G.; Tang, M.; Sun, L.; Chen, Y.; Luo, C. Multilayer Coatings of Periodically Co-Deposited Graphene and Ag Substrate: Improving the Electrified Friction Interface by Modifying the Strength-Ductility Combination. *Surf. Coat. Technol.* **2024**, *482*, 130667. [CrossRef]
9. Huang, W.; Kong, L.; Wang, X. Electrical Sliding Friction Lubricated with Ionic Liquids. *Tribol. Lett.* **2017**, *65*, 17. [CrossRef]
10. Cao, Z.; Xia, Y.; Ge, X. Conductive Capacity and Tribological Properties of Several Carbon Materials in Conductive Greases. *Ind. Lubr. Tribol.* **2016**, *68*, 577–585. [CrossRef]
11. Si, L.; Pan, Y.; Zhang, X.; Wang, J.; Yao, J.; Wang, Y.; Liu, F.; He, F. Tribological Properties of Metallic Nanoparticles as Lubricant Additives under the Applied Electric Currents. *Ind. Lubr. Tribol.* **2018**, *70*, 1714–1720. [CrossRef]
12. Feng, X.; Hu, C.; Xia, Y.; Wang, Y. Study on Conductivity and Tribological Properties of Polyaniline/Molybdenum Disulfide Composites in Lithium Complex Grease. *Lubr. Sci.* **2022**, *34*, 182–195. [CrossRef]
13. Reddy, A.B.; Shah, F.U.; Leckner, J.; Rutland, M.W.; Glavatskih, S. Ionic Liquids Enhance Electrical Conductivity of Greases: An Impedance Spectroscopy Study. *Colloids Surf. A Physicochem. Eng. Asp.* **2024**, *683*, 132875. [CrossRef]
14. Ye, C.; Liu, W.; Chen, Y.; Yu, L. Room-Temperature Ionic Liquids: A Novel Versatile Lubricant. *Chem. Commun.* **2001**, 2244–2245. [CrossRef]
15. Somers, A.; Howlett, P.; MacFarlane, D.; Forsyth, M. A Review of Ionic Liquid Lubricants. *Lubricants* **2013**, *1*, 3–21. [CrossRef]
16. Amiril, S.A.S.; Rahim, E.A.; Syahrullail, S. A Review on Ionic Liquids as Sustainable Lubricants in Manufacturing and Engineering: Recent Research, Performance, and Applications. *J. Clean. Prod.* **2017**, *168*, 1571–1589. [CrossRef]
17. Li, Z.; Mangolini, F. Recent Advances in Nanotribology of Ionic Liquids. *Exp. Mech.* **2021**, *61*, 1093–1107. [CrossRef]
18. Waheed, S.; Ahmed, A.; Abid, M.; Mufti, R.A.; Ferreira, F.; Bashir, M.N.; Shah, A.U.R.; Jafry, A.T.; Zulkifli, N.W.; Fattah, I.M.R. Ionic Liquids as Lubricants: An Overview of Recent Developments. *J. Mol. Struct.* **2024**, *1301*, 137307. [CrossRef]
19. Shen, H.-Y.; Judeh, Z.M.A.; Ching, C.B. Selective Alkylation of Phenol with Tert-Butyl Alcohol Catalyzed by [Bmim]PF_6. *Tetrahedron Lett.* **2003**, *44*, 981–983. [CrossRef]
20. Zhou, F.; Liang, Y.; Liu, W. Ionic Liquid Lubricants: Designed Chemistry for Engineering Applications. *Chem. Soc. Rev.* **2009**, *38*, 2590. [CrossRef]
21. Wijanarko, W.; Khanmohammadi, H.; Espallargas, N. Ionic Liquids as Boundary Additives in Water-Based and PAO Lubricants. *Friction* **2021**, *10*, 1405–1423. [CrossRef]
22. Cao, Z.; Xia, Y.; Chen, C.; Zheng, K.; Zhang, Y. Polyaniline as an Additive towards Improving Tribological Properties and Anti-Corrosion Performance of Ionic Liquids-Based Greases. *Ind. Lubr. Tribol.* **2020**, *72*, 851–856. [CrossRef]
23. Liu, X.; Zhou, F.; Liang, Y.; Liu, W. Benzotriazole as the Additive for Ionic Liquid Lubricant: One Pathway towards Actual Application of Ionic Liquids. *Tribol. Lett.* **2006**, *23*, 191–196. [CrossRef]
24. Cai, M.; Liang, Y.; Zhou, F.; Liu, W. Tribological Properties of Novel Imidazolium Ionic Liquids Bearing Benzotriazole Group as the Antiwear/Anticorrosion Additive in Poly(Ethylene Glycol) and Polyurea Grease for Steel/Steel Contacts. *ACS Appl. Mater. Interfaces* **2011**, *3*, 4580–4592. [CrossRef]

25. Yu, Q.; Yang, Z.; Huang, Q.; Lv, H.; Zhou, K.; Yan, X.; Wang, X.; Yang, W.; Zhou, C.; Yu, B.; et al. Lignin Composite Ionic Liquid Lubricating Material as a Water-Based Lubricating Fluid Additive with Excellent Lubricating, Anti-Wear and Anti-Corrosion Properties. *Tribol. Int.* **2022**, *174*, 107742. [CrossRef]
26. Zhang, C.; Yang, Z.; Huang, Q.; Wang, X.; Yang, W.; Zhou, C.; Yu, B.; Yu, Q.; Cai, M.; Zhou, F. Lignin Composite Ionic Liquid Lubricants with Excellent Anti-Corrosion, Anti-Oxidation, and Tribological Properties. *Friction* **2023**, *11*, 1239–1252. [CrossRef]
27. Fan, X.; Xia, Y.; Wang, L. Tribological Properties of Conductive Lubricating Greases. *Friction* **2014**, *2*, 343–353. [CrossRef]
28. Jech, M.; Miranda-Medina, M.L.; Wopelka, T.; Tomastik, C.; Gachot, C. Effect of Sliding on the Relation of Tribofilm Thickness and Wear. *Lubricants* **2023**, *11*, 72. [CrossRef]
29. Liu, D.-L.; Cao, S.; Zhang, S.; Xu, J. Lubrication Film Thickness Calculation from Contact Resistance Measurement in Point Contact. *Ind. Lubr. Tribol.* **2016**, *68*, 176–182. [CrossRef]
30. Xie, G.; Guo, D.; Luo, J. Lubrication under Charged Conditions. *Tribol. Int.* **2015**, *84*, 22–35. [CrossRef]
31. Chen, W.; Feng, Y.; Wan, Y.; Zhang, L.; Yang, D.; Gao, X.; Yu, Q.; Wang, D. Investigation on Anti-Wear and Corrosion-Resistance Behavior of Steel-Steel Friction Pair Enhanced by Ionic Liquid Additives under Conductive Conditions. *Tribol. Int.* **2023**, *177*, 108002. [CrossRef]
32. Dong, R.; Bao, L.; Yu, Q.; Wu, Y.; Ma, Z.; Zhang, J.; Cai, M.; Zhou, F.; Liu, W. Effect of Electric Potential and Chain Length on Tribological Performances of Ionic Liquids as Additives for Aqueous Systems and Molecular Dynamics Simulations. *ACS Appl. Mater. Interfaces* **2020**, *12*, 39910–39919. [CrossRef] [PubMed]
33. Yamashita, T.; Hayes, P. Analysis of XPS Spectra of Fe^{2+} and Fe^{3+} Ions in Oxide Materials. *Appl. Surf. Sci.* **2008**, *254*, 2441–2449. [CrossRef]
34. Li, J.; Fu, L.; Xu, Z.; Zhu, J.; Yang, W.; Li, D.; Zhou, L. Electrochemical Properties of Carbon-Wrapped FeF_3 Nanocomposite as Cathode Material for Lithium Ion Battery. *Electrochim. Acta* **2018**, *281*, 88–98. [CrossRef]
35. Song, Z.; Fan, M.; Liang, Y.; Zhou, F.; Liu, W. Lithium-Based Ionic Liquids: In Situ-Formed Lubricant Additive Only by Blending. *Tribol. Lett.* **2013**, *49*, 127–133. [CrossRef]
36. Li, Y.-Y.; Liu, C.; Chen, L.; Wu, X.-Z.; Zhou, P.-F.; Shen, X.-Y.; Zhou, J. Multi-Layered Fluorinated Graphene Cathode Materials for Lithium and Sodium Primary Batteries. *Rare Met.* **2023**, *42*, 940–953. [CrossRef]
37. Thibeau, R.J.; Brown, C.W.; Heidersbach, R.H. Raman Spectra of Possible Corrosion Products of Iron. *Appl. Spectrosc.* **1978**, *32*, 532–535. [CrossRef]
38. Li, Y.-S.; Jang, S.; Khan, A.M.; Martin, T.V.; Ogrinc, A.L.; Wang, Q.J.; Martini, A.; Chung, Y.-W.; Kim, S.H. Possible Origin of D- and G-Band Features in Raman Spectra of Tribofilms. *Tribol. Lett.* **2023**, *71*, 57. [CrossRef]
39. Yao, J.L.; Ren, B.; Huang, Z.F.; Cao, P.G.; Gu, R.A.; Tian, Z.-Q. Extending Surface Raman Spectroscopy to Transition Metals for Practical Applications IV. A Study on Corrosion Inhibition of Benzotriazole on Bare Fe Electrodes. *Electrochim. Acta* **2003**, *48*, 1263–1271. [CrossRef]
40. Cao, P.G.; Yao, J.L.; Zheng, J.W.; Gu, R.A.; Tian, Z.Q. Comparative Study of Inhibition Effects of Benzotriazole for Metals in Neutral Solutions As Observed with Surface-Enhanced Raman Spectroscopy. *Langmuir* **2002**, *18*, 100–104. [CrossRef]
41. Yuan, Y.-X.; Han, S.-Y.; Wang, M.; Yao, J.-L.; Gu, R.-A. Raman Spectroscopic Studies on Surface Coordination Mechanism of Benzotriazole and Triphenylphosphine with Metals. *Vib. Spectrosc.* **2009**, *51*, 162–167. [CrossRef]
42. Li, C.; Wang, G.; Han, Q.; Feng, G.; Wang, L.; Wang, S. Effects of Current-Carrying Conditions on Lubrication and Tribological Performance of Ionic Liquid. *J. Mol. Liq.* **2022**, *367*, 120471. [CrossRef]
43. Cao, Z.; Xia, Y.; Liu, L.; Feng, X. Study on the Conductive and Tribological Properties of Copper Sliding Electrical Contacts Lubricated by Ionic Liquids. *Tribol. Int.* **2019**, *130*, 27–35. [CrossRef]
44. Feng, Y.; Cheng, Y.F. Inhibitive Performance of Benzotriazole for Steel Corrosion Studied by Electrochemical and AFM Characterization. *J. Mater. Eng. Perform.* **2015**, *24*, 4997–5001. [CrossRef]
45. Khadom, A.A. Protection of Steel Corrosion Reaction by Benzotriazoles: A Historical Background. *J Fail. Anal. Preven.* **2015**, *15*, 794–802. [CrossRef]
46. Petrunin, M.; Maksaeva, L.; Gladkikh, N.; Makarychev, Y.; Maleeva, M.; Yurasova, T.; Nazarov, A. Thin Benzotriazole Films for Inhibition of Carbon Steel Corrosion in Neutral Electrolytes. *Coatings* **2020**, *10*, 362. [CrossRef]
47. Ge, X.; Wu, X.; Shi, Q.; Liu, Y.; Liang, H. Influence of Electrical Stimulation on the Friction Performance of $LiPF_6$-Based Ionic Liquids. *Lubricants* **2024**, *12*, 167. [CrossRef]

Disclaimer/Publisher's Note: The statements, opinions and data contained in all publications are solely those of the individual author(s) and contributor(s) and not of MDPI and/or the editor(s). MDPI and/or the editor(s) disclaim responsibility for any injury to people or property resulting from any ideas, methods, instructions or products referred to in the content.